SPECTRA OF SOLAR IMPULSIVE ELECTRON EVENTS OBSERVED NEAR EARTH

SÄM KRUCKER[1], P. H. OAKLEY[1,2], AND R. P. LIN[1,3]

[1] Space Sciences Laboratory, University of California, Berkeley, CA 94720-7450, USA; krucker@ssl.berkeley.edu
[2] Department of Astrophysical and Planetary Sciences, University of Colorado, Boulder, CO 80309-0391, USA
[3] Department of Physics, University of California, Berkeley, CA 94720-7300, USA

ABSTRACT

A statistical survey of the spectral shapes of 62 solar impulsive electron events detected in the ~ 1 to 300 keV range near Earth by the three-dimensional Plasma and Energetic Particles experiment on the *WIND* spacecraft is presented. The electron peak flux spectra generally show a broken power-law dependence with a steepening above ~ 60 keV. The break in the spectrum is pronounced with averaged power-law indices below and above the break of $\delta_{low} = 1.9 \pm 0.3$ and $\delta_{high} = 3.6 \pm 0.7$, respectively, and an averaged ratio $\delta_{low}/\delta_{high}$ of 0.54 with a standard deviation of 0.09. Two correlations are found: (1) δ_{low} and δ_{high} are linearly correlated (correlation coefficient of 0.61), (2) The peak fluxes around the break energy and δ_{low} are anticorrelated (coefficient 0.74), with larger events having flatter spectra below the break. Whether the observed spectral breaks are direct signatures of the solar acceleration processes or whether they are due to transport effects from the Sun to Earth is currently not understood.

Key words: Sun: flares – Sun: particle emission – Sun: radio radiation – Sun: X-rays, gamma rays

Online-only material: color figures

1. INTRODUCTION

The Sun is the most energetic natural electron accelerator in our solar system, producing electrons with energies of up to hundreds of MeV. It is generally agreed that the energy for particle acceleration comes from the solar magnetic field, however the details of the acceleration mechanisms are not understood. Remote sensing, hard X-ray observations of the bremsstrahlung emission by these electrons provide the most direct diagnostics of electron spectra near the Sun. The electron spectra derived from these observations show power-law or broken-power shapes (e.g., Lin & Schwartz 1987). It is speculated that the observed breaks in the X-ray spectrum are direct signatures of the acceleration mechanism. However, many processes such as nonuniform ionization (e.g., Kontar et al. 2002), albedo Compton backscattering (e.g., Kašparová et al. 2007), and self-induced electric fields produced by beam electrons during their precipitation (e.g., Zharkova & Gordovskyy 2006) could influence the spectral shape as well. The observed spectral breaks therefore do not necessarily have to be a signature of the acceleration mechanism.

Accelerated electrons on magnetic field lines open to interplanetary space can escape the Sun before they lose their energy and slow down. In situ observations in the heliosphere therefore provide the opportunity to directly detect solar flare accelerated electrons (e.g., van Allen & Krimigis 1965; Anderson & Lin 1966). The in situ observed spectral shapes also show broken power laws (e.g., Lin et al. 1982). The relatively similar electron spectra observed with remote sensing and in situ observations suggest that transport effects cannot be that important. However, the spectral shape of the in situ observed electrons could also be altered by an energy-dependent escape and/or transport effects. In particular, wave–particle interactions could distort the spectrum significantly (e.g., Kontar 2001).

Here we present a statistical survey of impulsive electron events detected by the three-dimensional Plasma and Energetic Particles experiment (3DP; Lin et al. 1995) instrument onboard the *WIND* spacecraft that covers the energy range from ~ 1 keV up to 500 keV.

2. OBSERVATIONS

The 3DP experiment provides electron measurements from solar wind energies up to the semirelativistic energy range. Impulsive electron events are best detected with the electrostatic analyzers (EESAs) from ~ 0.5 keV to 27 keV, and the solid-state telescopes (SSTs) from 23 keV to ~ 300 keV. Standard *WIND* software has been used to calibrate and analyze the data. The peak flux spectra presented here were produced by summation over angular bins (omnidirectional flux). The three-dimensional capability of the instrument made it possible to avoid summing over bins contaminated by solar soft X-rays or other background emissions.

For the survey presented in Section 2.1, only events with the best data quality and counting statistics were used. First, the *WIND*/3DP observations between 1994 November and 2005 December were searched for solar impulsive electron events that have (1) an impulsive onset, (2) a clear velocity dispersion, (3) a beamed pitch angle distribution, and (4) no instrumental artifacts (such as penetrating protons, high background, and data gaps). Furthermore, only events observed over a wide energy range from a few keV up to 300 keV were used to ensure that the spectral shape could be fitted over the largest energy range possible. These criteria reduced the number of events to 62. Most of the discarded events were only observed by the SST above 23 keV (208 out of 319), but not by the less sensitive electrostatic analyzers. A smaller number of events (49 out of 319) were discarded because they are only seen at lower energies. Sections 2.2 and 2.3 present statistical studies of events seen only at high or low energies.

2.1. Events Seen from ∼1 keV up to ∼ 300 keV

Figure 1 shows an example of a typical impulsive electron event observed from ~ 1 keV to 500 keV and its peak flux spectrum. The two instruments (EESA and SST) generally
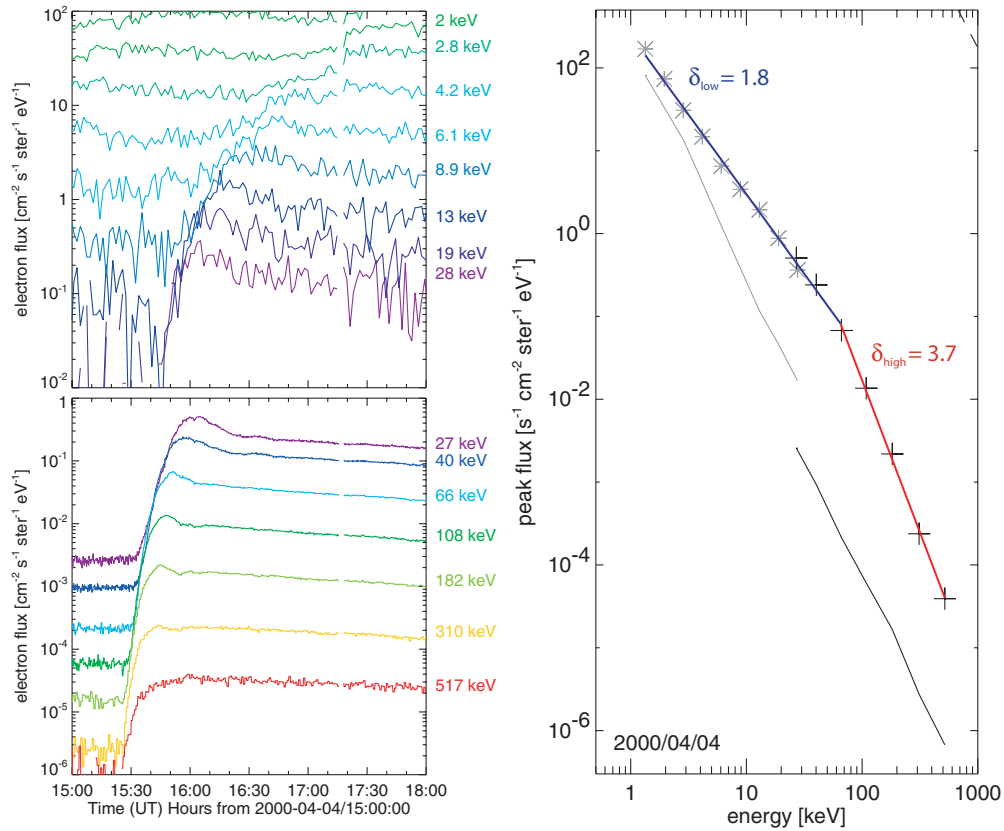
Figure 1. Example of a typical solar impulsive electron event observed from the keV range up to ~ 500 keV. Left: time profiles at different energies as indicated. The top panel shows data from the electrostatic analyzer (EESA-H) and the bottom panel shows data from the SST. Note the much higher sensitivity of SST. Right: derived electron peak flux spectrum of the same event. EESA-H data are shown in gray (asterisk), while the SST measurements are given in black (crosses). The thin curves below give an estimate of the background emission. The red and blue curves are the power-law fits to the data, with a pronounced break around 60 keV.

(A color version of this figure is available in the online journal.)

provide good agreement around ~ 25 keV (e.g., Lin et al. 1996; Ergun et al. 1998), so that no bias is introduced. The peak flux spectrum is constructed by taking the peak flux in each energy channel (due to velocity dispersion, the peak times are later for lower energies). The peak flux spectrum would be representative of the injection spectrum if the scattering in the interplanetary medium has the same spatial dependence for all electron energies (the intensity of the scattering can vary with energy; see Lin 1974 for details). The electron spectrum shown can be represented by a broken power law with a steeper (softer) spectrum at higher energy. The break in the spectrum is around ~ 60 keV and is significantly steeper at higher energies. The values of the power-law index below (δ_{low}) and above (δ_{high}) the break are 1.8 and 3.7, respectively. Error estimates on the peak flux are difficult to obtain. Therefore, the error estimates of the fit parameters are not well determined, but can be roughly estimated to be ~ 0.2.

All the electron spectra in the survey are well represented by a broken power law with a steepening at higher energy in the same way as the example shown in Figure 1. The averaged values and standard deviations of power-law indices below and above the break are $\delta_{low} = 1.9 \pm 0.3$ and $\delta_{high} = 3.6 \pm 0.7$, respectively (Figure 2(a)). The break energies are typically around ~ 60 keV and can be as low as 30 keV and occasionally above 100 keV (Figure 2(b)). The break energy seems not to be correlated with the power-law indices (Figure 2(d)), nor with the peak flux at 50 keV, i.e., the peak flux near the break energy (Figure 2(e)). However, δ_{low} is linearly correlated with the logarithm of the peak flux at 50 keV (Figure 2(f)). The correlation is clearly

seen for peak flux values above 0.02 (with correlation coefficient of 0.74), but not for smaller values. The lack of correlation for small events could possibly be a selection effect, as small events are only seen for flat spectra (see Section 2.3 for further discussion). The correlation between δ_{high} and the peak flux is much less pronounced, if it exists at all. The knee in the spectra is pronounced, with differences in the power-law indices typically around 1.7 ± 0.5 (Figure 2(h)). The scatter plot of δ_{low} and δ_{high} over all events reveals a linear correlation with a correlation coefficient of 0.61 (Figure 2(g)). A linear fit provides $\delta_{low} = (0.31 \pm 0.04)$ and $\delta_{high} + (0.8 \pm 0.2)$ with correlation coefficient of 0.62. The ratio $\delta_{low}/\delta_{high}$ falls in a rather narrow range with an averaged value of 0.54 and a standard deviation of 0.09 (Figure 2(i)).

2.2. Events Only Seen Above 23 keV

Most of the discarded events are only seen by SST above 23 keV. Since only seven energy channels are available for these events, a broken power-law fit does not provide reliable results. However, fitting the four energy channels above 100 keV with a power law gives reliable measurements of δ_{high} (Figure 3(b)). A single power-law fit above 100 keV for 208 events provides $\delta_{high} = 3.5 \pm 0.6$, consistent with the slopes found for the events with full energy coverage. For most of the events, the observed peak fluxes below 100 keV are clearly smaller than the extrapolated power-law fit to the >100 keV data suggesting the existence of a break (Figure 3(b)). These findings suggest that the events seen only above 23 keV are likely to be of the same kind as events seen over the entire energy range.
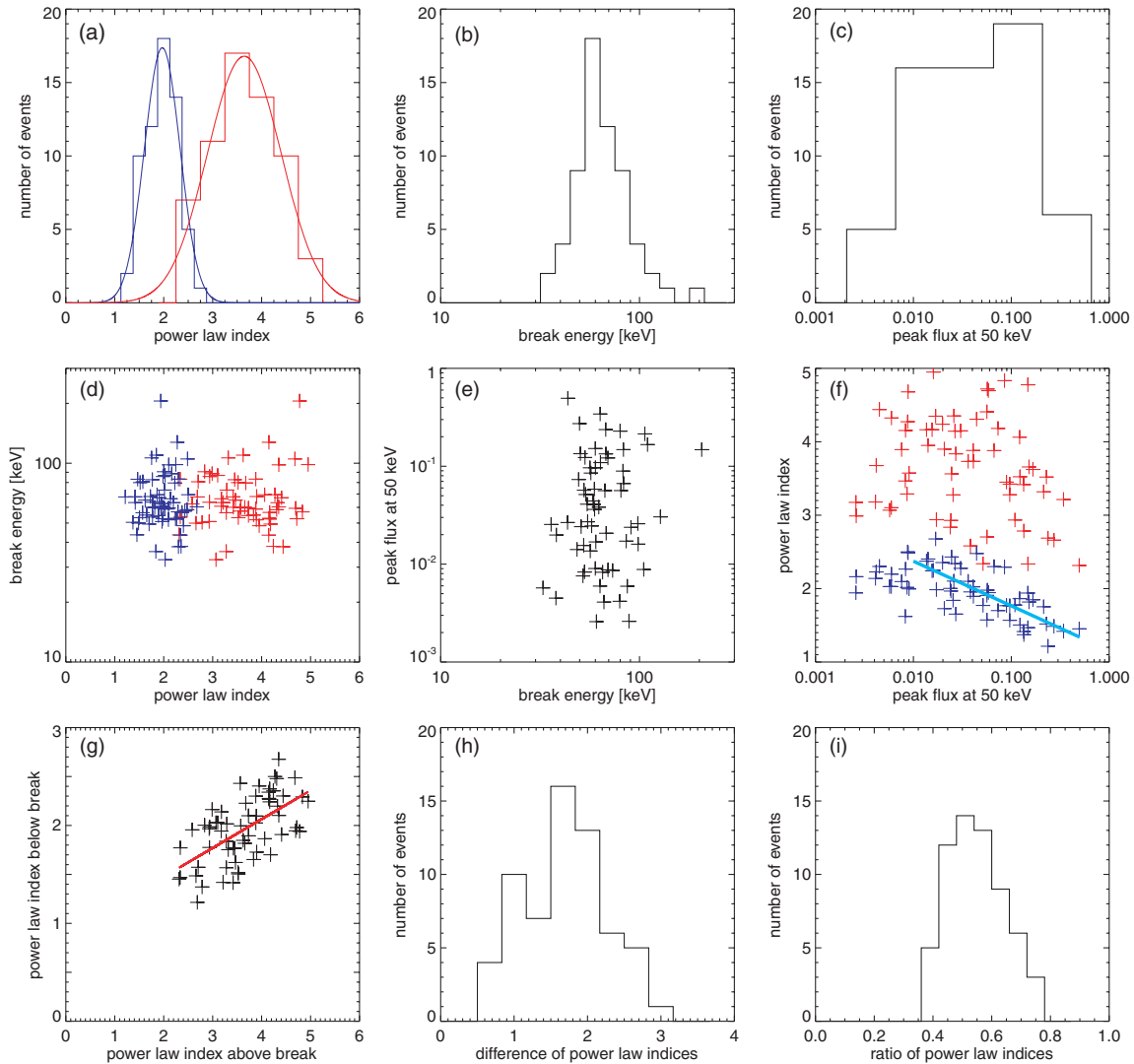
Figure 2. Statistical results of the derived spectral parameters. (a) Histogram of the power-law index below δ_{low} (blue) and above δ_{high} (red) the break energy. The distributions are fitted with a Gaussian, giving averaged values of 1.9 and 3.6 with an FWHM of 0.4 and 0.8, respectively. (b) Histogram of the break energies. (c) Histogram of the peak flux at 50 keV (i.e., peak flux near the break energy; units are cm^{-2} s^{-1} $ster^{-1}$ eV^{-1}). (d–g) Scatter plot of the spectral parameters as indicated (δ_{low} and δ_{high} are again represent by blue and red); the light blue and the red lines in (f) and (g) are linear fits to the data. The last two panels show the histogram of the difference $\delta_{low} - \delta_{high}$ (h) and the ratio $\delta_{low}/\delta_{high}$ (i) of the power-law index below and above the break, respectively.

(A color version of this figure is available in the online journal.)

2.3. Events Only Seen Below ∼ 20 keV

We also analyzed 49 events that were only seen by the less sensitive EESA at low energies, but not by the more sensitive SST above 23 keV (Figure 3(c)). These events are generally best observed around a few keV and are not well correlated with the occurrence of solar X-ray flares (Potter et al. 1980), but are well associated with interplanetary radio type III bursts (e.g., Gosling et al. 2003). Single power-law fits between ∼ 1 and ∼ 10 keV reveal averaged values for the power-law index around 3.2 with a standard deviation of 0.4 (Figure 4(a)). These values are similar to what is reported by Gosling et al. (2003; 3.0–3.8), but slightly lower than what is given in Potter et al. (1980; δ between 3.5 and 5). In any case, δ_{low} for events seen at low energies only are much larger than for the events seen over the entire range, and the two distributions of δ_{low} have almost no overlap (Figure 4(a)). Around 1 keV, these events are about as intense as the events seen over the entire energy range (Figure 4(b)). Extrapolated to 30 keV (Figure 4(c)), the peak fluxes are expected to be below the typical background

flux of SST (a few times 10^{-3} s^{-1} cm^{-2} $ster^{-1}$ eV^{-1} or larger, depending on pre-event emission). This allows the possibility that events seen only at low energies might be of the same kind as events seen over the entire energy range, but with a steeper spectrum. This might also explain the poor correspondence of the < 1 keV events studied by Gosling et al. (2003) with events observed by EPAM (Gold et al. 1998) above ∼ 40 keV (Haggerty & Roelof 2002). If the correlation between δ_{low} and δ_{high} is also valid for the events seen only at low energies, δ_{high} would be expected to be extremely steep with values between 6 and 8. The low number of high-energy electrons in these events might explain the observed lack of association with hard X-ray flare emission. However, the presented spectral study cannot exclude that low-energy events are a different class of events as suggested by Potter et al. (1980).

3. COMPARISON WITH HARD X-RAY OBSERVATIONS

Near the Sun, nonthermal electrons produce bremsstrahlung emissions in the hard X-ray range. Inversion of the observed
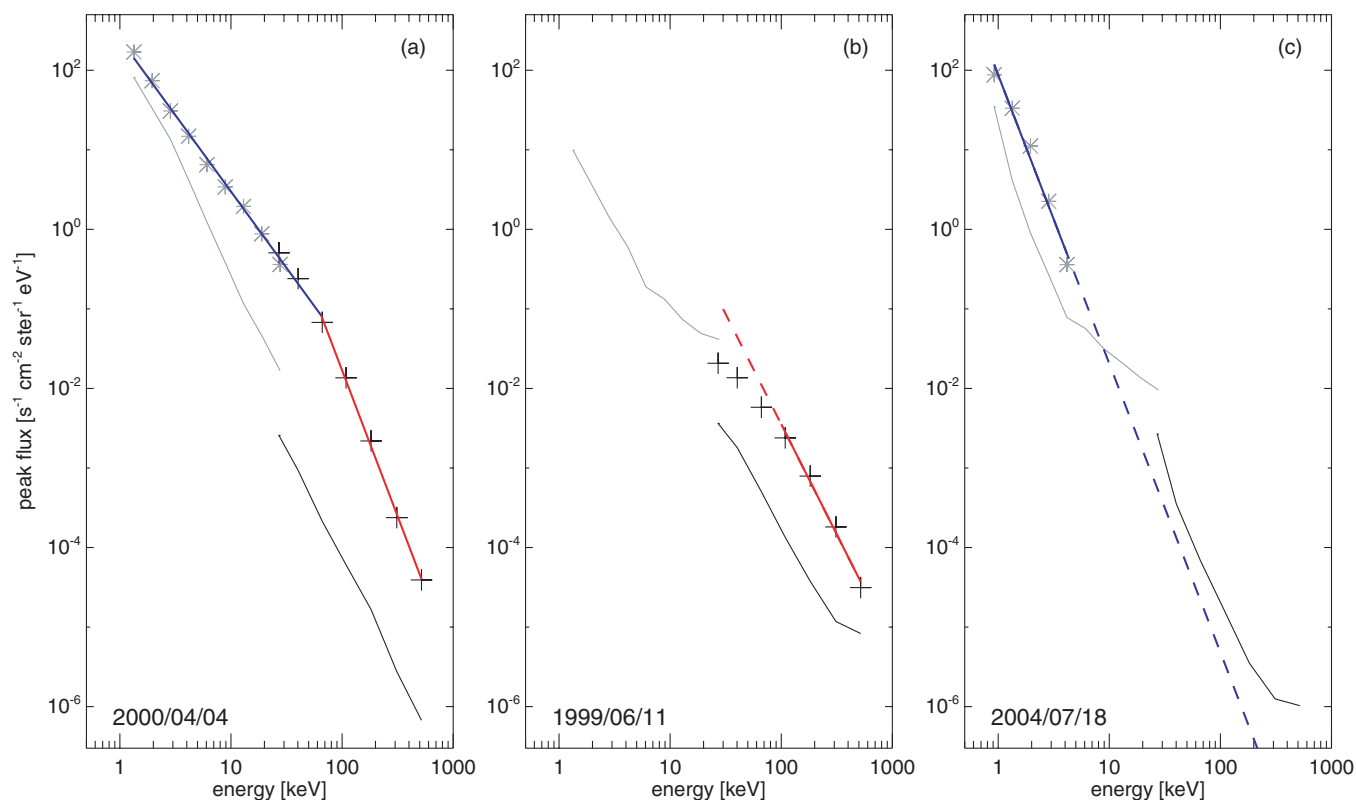
Figure 3. Example of spectra observed over different energy ranges (same format as for Figure 1). (a) Events seen over the entire energy range (same event as shown in Figure 1). (b) Event seen only at high energies. The red curve is a power-law fit to the > 100 keV data (δ_{high} = 2.8). Below 100 keV, the observed peak fluxes are smaller than the extrapolated power-law fit (dashed line), indicating the existence of a break. (c) Event seen only at low energies. The blue curve is a power-law fit to the data (δ_{high} = 3.6). The extrapolated fit to higher energies shows that the event is too weak to be seen with SST above 23 keV.

(A color version of this figure is available in the online journal.)
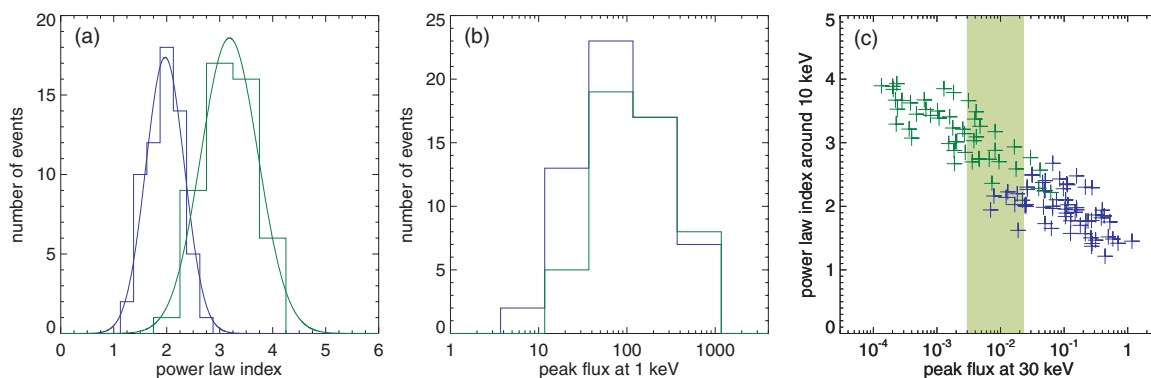
Figure 4. Statistical results of events observed only below 20 keV (green corresponds to the sample of events seen only below 20 keV and blue represents the events also seen above 27 keV by SST). (a) Histogram of the power-law indices δ_{low}. The green Gaussian fit gives averaged values of 3.2 with an FWHM of 0.5. (b) Histogram of the peak flux at 1 keV. (c) Scatter plot of the peak flux at 30 keV (extrapolated fluxes for the events seen only at low energies) and δ_{low}. The light green area makes the detection limit of SST for a range of pre-event fluxes.

(A color version of this figure is available in the online journal.)

photon spectrum provides information on the spectrum of the nonthermal electrons. In this section, the electron spectra derived from hard X-ray observations are compared with in situ observed electron spectra. It is not the scope of this paper to compare individual events, but the averaged properties are investigated.

At the peak of the hard X-ray emission, hard X-ray photon spectra of the flare generally show broken power-law spectra with a similar break energy as the in situ observed electron spectra (e.g., Lin & Schwartz 1987; Dulk et al. 1992; Krucker & Lin 2002; Conway et al. 2003). Gaussian fits to the histograms of spectral indices of the photon spectrum published by Dulk

et al. (1992) give average values of $\gamma_{low} \sim 2.9 \pm 0.5$ and $\gamma_{high} \sim 4.4 \pm 0.7$. The reported break energies range from 30 keV up to 150 keV.

For the simple comparisons discussed here, the thick-target approximation is used in the inversion of the photon spectrum (e.g., Brown 1971). Above the break energy, the spectral shapes of the electron spectrum then become $\delta_{high}^{thick} = \gamma_{high} + 1$. The inversion below the break is more complicated because the hard X-ray emission below the break is partially produced by electrons above the break, and γ_{low} therefore deviates from the simple thick-target value, i.e., $\gamma_{low} > \gamma_{low}^{thick} = \delta_{low} - 1$. For a broken electron spectrum producing hard X-ray emission,

the break in the resulting photon spectrum is therefore less pronounced than in the electron spectrum, i.e., $\gamma_{\mathrm{high}} - \gamma_{\mathrm{low}} < \delta_{\mathrm{high}} - \delta_{\mathrm{low}}$ (see Holman et al. 2003 for an example). Statistical results of photon spectra by Dulk et al. (1992) report, on average, less-pronounced breaks with $\gamma_{\mathrm{high}} - \gamma_{\mathrm{low}}$ around ~ 1 than that which are reported here for electron spectra (Figure 2(h)). This suggests that the breaks in electron spectra could be equally pronounced for the hard X-ray–producing electrons as for the in situ observed electrons.

For the observed averaged photon spectral index above the break, γ_{high}, the derived electron spectra have spectral slopes of $\delta_{\mathrm{high}}^{\mathrm{thick}} = 5.4 \pm 0.7$. Hence, in the thick-target assumption, the spectra of the electrons producing the hard X-ray emissions at the Sun are much steeper/softer than the spectra of the electrons observed near 1 AU ($\delta_{\mathrm{high}} = 3.6 \pm 0.7$). Although it is difficult to imagine how the thin-target scenario could be realized, it is interesting to note that the thin-target approximation gives similar average spectral indices for the hard X-ray-producing electrons ($\delta_{\mathrm{high}}^{\mathrm{thin}} \sim 3.4 \pm 0.7$) as for the in situ observed values ($\delta_{\mathrm{high}} = 3.6 \pm 0.7$).

A further main difference between the flare electrons and the in situ observed electrons is the total number of electrons: The number of escaping electrons is only a very small fraction, of the order of 0.5%, compared to the number of electrons needed to produce the observed hard X-ray emission (e.g., Lin & Hudson 1971).

In summary, the statistical properties of spectra near the Sun and near Earth show two main differences: (1) the number of escaping electrons is much lower, and (2) the escaping electrons have flatter/harder spectra. Hence, despite the fact that broken power-law spectra with similar break energies are observed for both, the electron population at the Sun and near Earth are quiet different and might be produced by different acceleration mechanisms; or, the escape from the Sun is energy-dependent. However, when only considering events with close temporal correlation between the hard X-ray burst and the in situ electron events, the so-called prompt events (e.g., Krucker et al. 1999), the hard X-ray, and the in situ observed spectral index are found to be correlated (Krucker et al. 2007, 2008). Hence, for the subset of prompt events, a single electron population is likely to be responsible for both the hard X-ray emission and the escaping electrons.

4. SUMMARY

The statistical results presented in this survey agree with earlier findings that in situ observed electron events generally show broken power-law spectra. A statistical study by Lin et al. (1982) of nine events seen in the 10 keV to the 10 MeV range reports δ_{low} between 0.6 and 2.0 and δ_{high} between 2.4 and 4.3, comparable to the values reported here ($\delta_{\mathrm{low}} = 1.9 \pm 0.3$ and $\delta_{\mathrm{high}} = 3.6 \pm 0.7$). For some events, an additional steepening above a few MeV is reported as well (for observations of electron spectra at higher, > 1 MeV, energies; also see Moses et al. 1989 and Mewaldt et al.

2005). The break energies given in Lin et al. (1982) are slightly higher (~ 100 to ~ 200 keV) than what is reported here, however, the difference is due to different fitting ranges. Fitting the spectra shown in Figure 5 of Lin et al. (1982) only below 500 keV gives break energy below 100 keV. Hence, using different fitting ranges introduces a slight bias. Lin et al. (1982) also report a correlation between electron flux and δ_{low} (their Figure 11), similar to what is found in this study (Figure 2(f)).

The origin of the observed broken power-law spectra is not presently understood. The breaks could by a direct signature of the acceleration process or they could be produced by a secondary process, such as escape from the acceleration region or by transport effects. Collisional losses alone cannot produce the observed breaks as low-energy electrons should be lost entirely, producing a rollover and not a break (e.g., Lin 1985). Wave–particle interactions could change the shape of the accelerated electron spectrum and produce breaks, as energy from the electrons can be lost to waves (e.g., Kontar 2001). Presently these questions are open and pose a challenge to the theory of particle acceleration and transport.

REFERENCES

Anderson, K. A., & Lin, R. P. 1966, Phys. Rev. Lett., 16, 1121
Brown, J. C. 1971, Sol. Phys., 18, 489
Conway, A. J., Brown, J. C., Eves, B. A. C., & Kontar, E. 2003, A&A, 407, 725
Dulk, G. A., Kiplinger, A. L., & Winglee, R. M. 1992, ApJ, 389, 756
Ergun, R. E., et al. 1998, ApJ, 503, 435
Gold, R. E., et al. 1998, Space Sci. Rev., 86, 541
Gosling, J. T., Skoug, R. M., & McComas, D. J. 2003, Geophys. Res. Lett., 30, 130000
Haggerty, D. K., & Roelof, E. C. 2002, ApJ, 579, 841
Holman, G. D., Sui, L., Schwartz, R. A., & Emslie, A. G. 2003, ApJ, 595, L97
Kašparová, J., Kontar, E. P., & Brown, J. C. 2007, A&A, 466, 705
Kontar, E. P. 2001, Sol. Phys., 202, 131
Kontar, E. P., Brown, J. C., & McArthur, G. K. 2002, Sol. Phys., 210, 419
Krucker, S., Kontar, E. P., Christe, S., & Lin, R. P. 2007, ApJ, 663, L109
Krucker, S., Larson, D. E., Lin, R. P., & Thompson, B. J. 1999, ApJ, 519, 864
Krucker, S., & Lin, R. P. 2002, Sol. Phys., 210, 229
Krucker, S., Saint-Hilaire, P., Christe, S., White, S. M., Chavier, A. D., Bale, S. D., & Lin, R. P. 2008, ApJ, 681, 644
Lin, R. P. 1974, IAU Symp., 57, Coronal Disturbances, ed. G. A. Newkirk (Dordrecht: Reidel), 201
Lin, R. P. 1985, Sol. Phys., 100, 537
Lin, R. P., & Hudson, H. S. 1971, Sol. Phys., 17, 412
Lin, R. P., Mewaldt, R. A., & van Hollebeke, M. A. I. 1982, ApJ, 253, 949
Lin, R. P., & Schwartz, R. A. 1987, ApJ, 312, 462
Lin, R. P., et al. 1995, Space Sci. Rev., 71, 125
Lin, R. P., et al. 1996, Geophys. Res. Lett., 23, 1211
Mewaldt, R. A., et al. 2005, J. Geophys. Res. (Space Phys.), 110, 9
Moses, D., Droege, W., Meyer, P., & Evenson, P. 1989, ApJ, 346, 523
Potter, D. W., Lin, R. P., & Anderson, K. A. 1980, ApJ, 236, L97
van Allen, J. A., & Krimigis, S. M. 1965, J. Geophys. Res., 70, 5737
Zharkova, V. V., & Gordovskyy, M. 2006, ApJ, 651, 553